Dyes and Pigments 185 (2021) 108886

Contents lists available at ScienceDirect

Dyes and Pigments

journal homepage: http://www.elsevier.com/locate/dyepig

Thien-2-yl substituted chlorins as photosensitizers for photodynamic therapy and photodynamic antimicrobial chemotherapy

Balaji Babu, Azole Sindelo, John Mack *, Tebello Nyokong **

Institute for Nanotechnology Innovation, Department of Chemistry, Rhodes University, Makhanda 6140, South Africa

ARTICLE INFO

Keywords:
Chorins
PDT
PACT
Singlet oxygen
Photophysics
Photosensitizer dye

ABSTRACT

The synthesis and characterization of *meso*-tetra(thien-2-yl)chlorin (**1**) and *meso*-tetra(5-bromothien-2-yl)chlorin (**2**) is reported. These dyes have red-shifted absorption maxima compared to those of the analogous *meso*-tetraphenylchlorin (**3**). **1** and **2** have Q bands at 660 and 664 nm, respectively, singlet oxygen quantum yields of 0.60 and 0.64 and exhibit good photostability. The triplet states were found to have lifetimes of 8.6 μs in N_2 purged DMF. Time-dependent cellular uptake of chlorins reached a maximum in MCF-7 cancer cells after 12 h. Upon irradiation with a Thorlabs M660L3 LED (280 mW cm^{-2}), **2** exhibited better photocytotoxicity with an IC_{50} value of 2.7 μM against MCF-7 cells. The 2′,7′-dichlorodihydrofluorescein diacetate (DCFDA) assay provided evidence for intracellular generation of reactive oxygen species. Photodynamic inactivation of bacteria by the chlorins was also studied. **2** exhibits better activity with log reduction values of 7.42 and 8.34 towards *Staphylococcus aureus* and *Escherichia coli*, respectively, under illumination for 60 min at 660 nm with a Thorlabs M660L3 LED (280 mW cm^{-2}). These results demonstrate that **2** is a promising candidate for future *in vivo* experiments and merits further in-depth investigation.

1. Introduction

Photodynamic therapy (PDT) is a non-invasive mode of treatment of cancer that requires a photosensitizer dye, light and molecular oxygen. When a photosensitizer dye is excited with light of an appropriate wavelength, it transfers its excited state energy by a Type II process to form highly reactive singlet oxygen species which can damage the tumour tissue [1–5]. Photofrin® (an oligomeric mixture of hematoporphyrin) was the first photosensitizer approved by the FDA as a PDT drug and is widely used for different types of cancer [6–9]. Chlorins, which are porphyrin analogues which contain one reduced exocyclic double bond, have recently gained considerable attention for use in PDT [10–12], since they have an intense absorption band that lies beyond 650 nm in the therapeutic window (620–1000 nm). Photosensitizer dyes that absorb at longer wavelength can facilitate penetration of laser light into tissues to a much deeper depth [10]. Chlorin-based photosensitizers such as Foscan® (*meso*-tetrahydroxyphenylchlorin, THPC) and mono-L-aspartyl chlorin e_6 (NPe_6) have already been approved for the treatment of head and neck cancers [13–15]. Photosensitizer dyes also work effectively against many bacterial infections through photodynamic antimicrobial chemotherapy (PACT). Singlet oxygen generated by a photosensitizer dye can disturb bacterial functions by reacting with its membrane units and internal structures. The key advantage of PACT is that while resistance can be developed against normal chemotherapeutic drugs, it is difficult to generate resistance against singlet oxygen [16].

The introduction of thiophene moieties and heavy atoms to photosensitizers is known to enhance the rate of intersystem crossing (ISC) and the generation of $^1O_2$ [17–19]. Tetrathienylporphyrins and their metal complexes have been the focus of considerable research interest due to their favorable photophysical and chemical properties, low dark toxicity and good photodynamic activity against MCF-7 cells [20–24]. The major drawback of these compounds is the absence of an intense absorption band at longer wavelength in the therapeutic window. Herein, we report the synthesis and characterization of *meso*-tetra(thien-2-yl)chlorin **1** and *meso*-tetra(5-bromothien-2-yl)chlorin **2** (Scheme 1) along with studies of their PDT activity against MCF-7 cells and PACT activity against both gram (+) (*Staphylococcus aureus*) and gram (−) (*Escherichia coli*) bacteria in comparison to *meso*-tetraphenylchlorin **3**.

* Corresponding author.
** Corresponding author.
E-mail addresses: j.mack@ru.ac.za (J. Mack), t.nyokong@ru.ac.za (T. Nyokong).

https://doi.org/10.1016/j.dyepig.2020.108886
Received 25 August 2020; Received in revised form 22 September 2020; Accepted 23 September 2020
Available online 28 September 2020

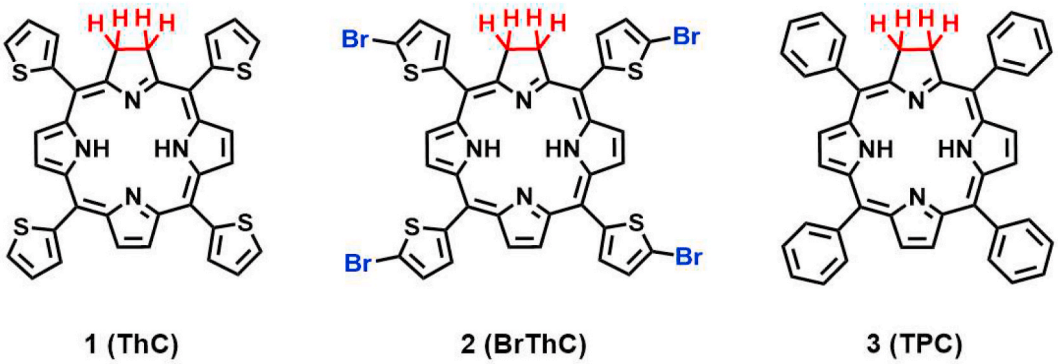

Scheme 1. (a) Molecular structures of chlorins **1**–**3**.

2. Experimental section

2.1. Materials

Benzaldehyde, thiophene-2-carboxaldehyde, 5-bromo-2-thiophenecarboxaldehyde, 2′,7′-dichlorofluorescein diacetate (DCFDA), Methylene blue, N-acetyl-L-cysteine (NAC), zinc tetraphenylporphyrin, 3-(4,5-dimethyl-2-thiazolyl)-2,5-diphenyl-2H-tetrazolium bromide (MTT) and Triton-X-100 were obtained from Sigma Aldrich. 5,10,15,20-Tetra (thien-2-yl)porphyrin (TTP, **4**), 5,10,15,20-tetra(5-bromo-2-thienyl) porphyrin (BrTTP, **5**) and 5,10,15,20-tetraphenylporphyrin (TPP, **6**) were prepared according to literature procedures [25,26]. All other reagents and solvents were purchased from commercial suppliers and were of analytical grade and used without any further purification. Cultures of MCF-7 cells were obtained from Cellonex®. 100 unit/mL penicillin−100 μg/mL streptomycin-amphotericin B and 10% (v/v) heat-inactivated fetal bovine serum were obtained from Biowest®. Dulbecco's modified Eagle's medium (DMEM) and Dulbecco's phosphate-buffered saline were purchased from Lonza®. Nutrient agar and agar bacteriological BBL Muller Hinton broth were obtained from Merck and prepared according to the specifications provided. *S. aureus* and *E. coli* were purchased from Davies Diagnostics and Microbiologic, respectively.

2.2. Equipment

UV–visible absorption spectra were recorded on a Shimadzu UV−2550 spectrophotometer, while a Varian Eclipse spectrofluorimeter was used to record the fluorescence emission spectra. Fluorescence lifetimes were measured using a time-correlated single-photon counting setup (TCSPC) fitted with an LDH-P-670 diode laser (Picoquant, 20 MHz, 44 ps pulse width). Triplet state lifetimes were determined in N_2 saturated DMF solutions at 500 nm using an Edinburgh Instruments LP980 spectrometer with a pump beam of 425 nm provided by an Ekspla NT-342B laser fitted with an OPO. MS data were obtained on a Bruker® AutoFLEX III Smart-beam TOF/TOF mass spectrometer in positive ion mode by using α-cyano-4-hydroxycinnamic acid as the matrix. Details of the instrumentation and procedures used for photostability experiments, cell studies, cellular uptake experiments, DCFDA assays and antimicrobial studies are provided as Supporting Information.

2.3. Synthesis

Chlorins **1**–**3** were synthesized from the corresponding porphyrin according to literature procedures (Scheme S1) [27]. The appropriate porphyrin (1 mmol), K_2CO_3 (10 mmol) and *p*-toluenesulfonylhydrazine (4 mmol) were dissolved in dry pyridine (50 mL) and refluxed for 12 h. The same amount of *p*-toluenesulfonylhydrazine was added every 4 h. The reaction was stopped when the peak at 730 nm starts to appear, which corresponds to a doubly reduced bacteriochlorin product. After reaction completion, the reaction mixture was cooled and extracted using chloroform. Trace amounts of *p*-chloranil were added to the chloroform layer until the band at 730 nm disappeared. The solvent was removed on a rotatory evaporator, and the crude product was loaded onto a silica gel column with chloroform as the eluent to give the chlorin derivative. **1**–**3** were characterized by ^{1}H NMR spectroscopy (Figs. S1–3) and MALDI-TOF MS (Figs. S4–9).

1. (0.33 g, yield: 51%), ^{1}H NMR ($CDCl_3$, 400 MHz): δ, ppm 8.82 (d, 2H, $J = 4.92$ Hz), 8.62 (s, 2H), 8.38 (d, 2H, $J = 4.84$ Hz), 7.91 (d, 1H, $J = 3.40$ Hz), 7.85 (d, 1H, $J = 5.36$ Hz), 7.81 (d, 2H, $J = 3.40$ Hz), 7.78 (d, 2H, $J = 5.28$ Hz), 7.70 (d, 2H, $J = 5.29$ Hz), 7.50–7.53 (m, 4Hz), 4.32 (s, 4H), 1.29 (s, 2H); MALDI-TOF MS: *m/z* for [M+H] = 640.15 (calc. 640.09); UV–Vis (DMF): 426, 522, 554, 607, 660 nm.

2. (0.44 g, yield: 46%), ^{1}H NMR (DMSO-d_6, 400 MHz): δ, ppm 8.94

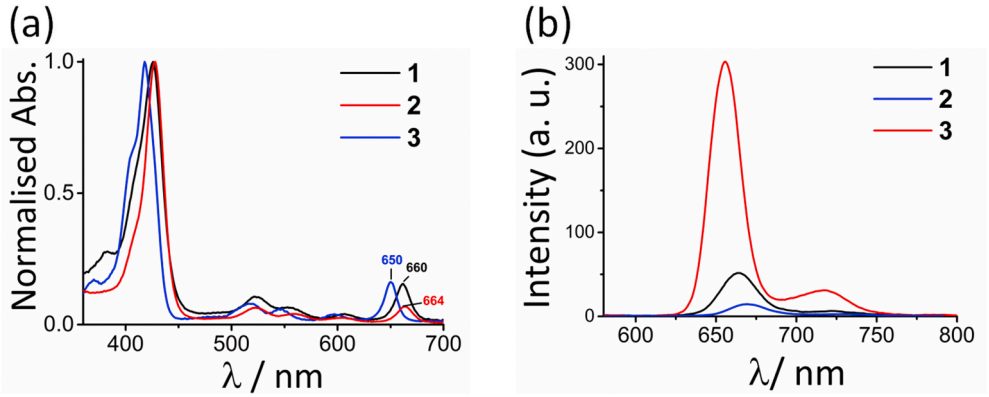

Fig. 1. (a) Absorption and (b) emission spectra of chlorins **1**–**3** in DMF.

Table 1
Selected photophysicochemical properties of **1**–**3** in DMF.

	1	2	3
λ_{max}	426, 522, 554, 607, 660	428, 523, 559, 607, 664	418, 517, 546, 597, 650
λ_{em} [a]	664, 722	670, 728	656, 718
Φ_F [b]	0.016	0.008	0.115
Φ_Δ	0.60	0.64	0.55
τ_T (μs) [c]	12.9 (±0.8)	8.6 (±0.2)	89.3 (±4.2)

[a] Excitation at the B (or Soret) band maxima
[b] ZnTPP = 0.033 in DMF
[c] N_2 purged.

(s, 1H), 8.62 (s, 2H), 8.85 (s, 1H), 8.63 (m, 1H), 8.51 (m, 2H), 8.40 (s, 1H), 8.12 (s, 1H), 8.61 (s, 1H), 7.92 (d, 1H, J = 3.24 Hz), 7.76 (s, 1H), 7.61 (m, 2H), 7.38 (m, 2H), 4.43 (s, 4H), 1.33 (s, 2H). MALDI-TOF MS: *m/z* for [M+H] = 957.00 (calc. 956.73), [M + H–Br] = 878.07 (calc. 877.54), [M + H–2Br] = 798.14 (calc. 798.65), [M + H–3Br] = 721.21 (calc. 720.75), [M + H–4Br] = 640.27 (calc. 640.86); UV–Vis (DMF): 428, 523, 559, 607, 664 nm.

3. (0.36 g, yield: 58%), ^{1}H NMR ($CDCl_3$, 400 MHz): δ, ppm 8.56 (d, 2H, J = 4.74 Hz), 8.42 (s, 2H), 8.17 (d, 2H, J = 4.74 Hz), 8.10 (d, 4H, J = 6.42 Hz), 7.87 (d, 4H, J = 7.92 Hz), 7.67 (m, 12H), 4.16 (s, 4H), 1.43 (s, 2H). MALDI-TOF MS: *m/z* for [M+H] = 616.32 (calc. 616.26); UV–Vis (DMF): 418, 517, 546, 597, 650 nm.

3. Results and discussion

3.1. Photophysical properties

The UV–visible absorption spectra of chlorins **1**–**3** in DMF are shown in Fig. 1a. All the chlorins have an intense B (or Soret) band between 418–428 nm and a Q band between 650–664 nm. As would normally be anticipated for chlorins, the Q band is more intense than those observed for tetraphenylporphyrins [10,11]. The presence of the *meso*-thien-2-yl rings of **1** and **2** shifts the absorption maxima at 660 and 664 nm significantly to the red compared to those of phenyl-substituted chlorin **3** at 650 nm (Table 1). This long-wavelength absorption band can hence be readily used for PDT in a manner that enables deeper tissue penetration.

The emission spectra of **1**–**3** exhibit two maxima between 664–728 nm when excited at their B band maxima (Fig. 1b). The fluorescence emission band maximum of **2** is more red-shifted than those of **1** and **3**. The calculated fluorescence quantum yield (Φ_F) values in DMF for **1** (0.016) and **2** (0.008) are lower than that of **3** (0.115). The decrease observed for **1** and **2** is due to a significant heavy-atom effect induced by the sulfur atoms of the *meso*-thien-2-yl groups. There is a further decrease in the Φ_F value for **2** compared to that of **1** due to the bromine atoms [28]. The heavy atoms facilitate ISC to the triplet state by spin-orbit coupling, thereby populating the triplet state and quenching the fluorescence [18,20].

3.2. Transient absorption spectra

The heavy atoms associated with the *meso*-aryl rings are known to populate the triplet manifold via ISC [20,21,28]. The T_1 state transfers its energy to molecular oxygen to form singlet oxygen ($^1O_2$) which is a key cytotoxic species [1,2]. Flash photolysis experiments were carried out in N_2-saturated DMF. The transient absorption spectrum of **1** is shown in Fig. 2a. The singlet depletion band in the 425–440 nm region corresponds to the chlorin B band. There is a triplet-triplet absorption band at 460 nm. The same trends are observed for **2** and **3** (Figs. S10 and S11). The triplet decay curves of **1**–**3** (Fig. 2b, S10, S11) show mono-exponential decay, with triplet state lifetime (τ_T) values of 12.9, 8.6, and 89.3 μs for **1**, **2**, and **3**, respectively. The decreased lifetimes for

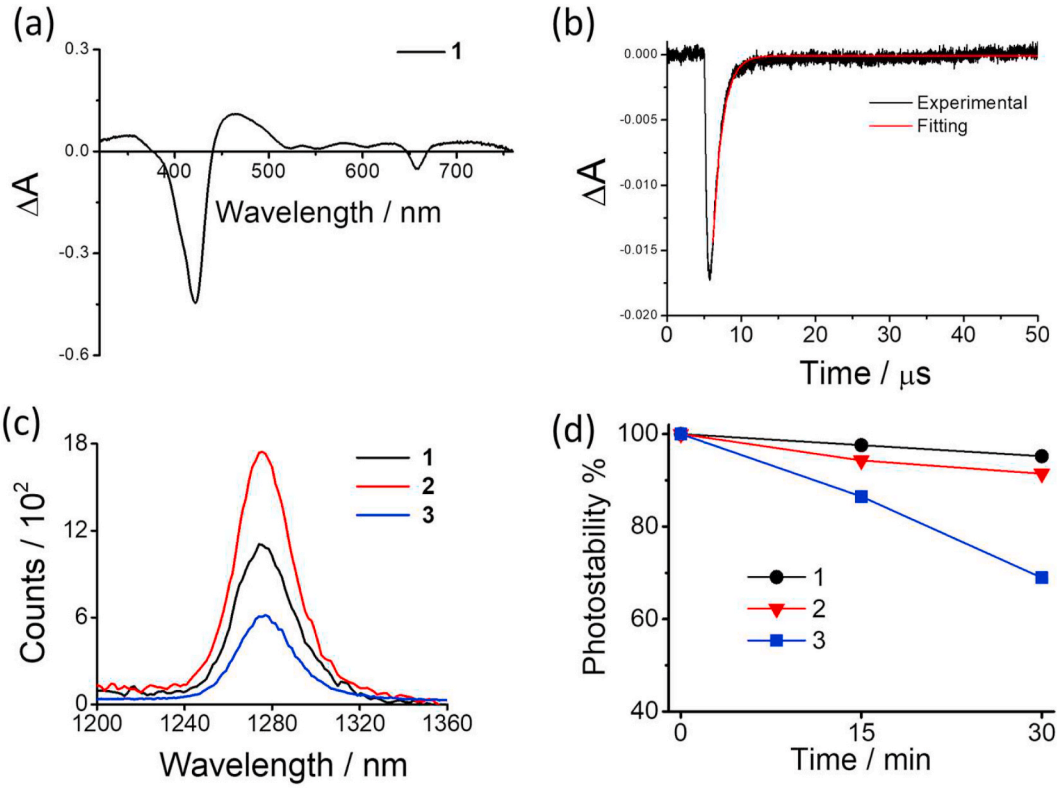

Fig. 2. (a) Transient absorption spectrum for **1** at 500 nm in nitrogen purged DMF; (b) The triplet absorption decay curve of **1** at 460 nm in DMF; (c) Singlet oxygen phosphorescence produced by **1**–**3** upon excitation at 420 nm in air-saturated DMF; and, (d) Photostability of **1**–**3** in aerated DMF solutions under irradiation at 660 nm with a Thorlabs M660L3 LED.

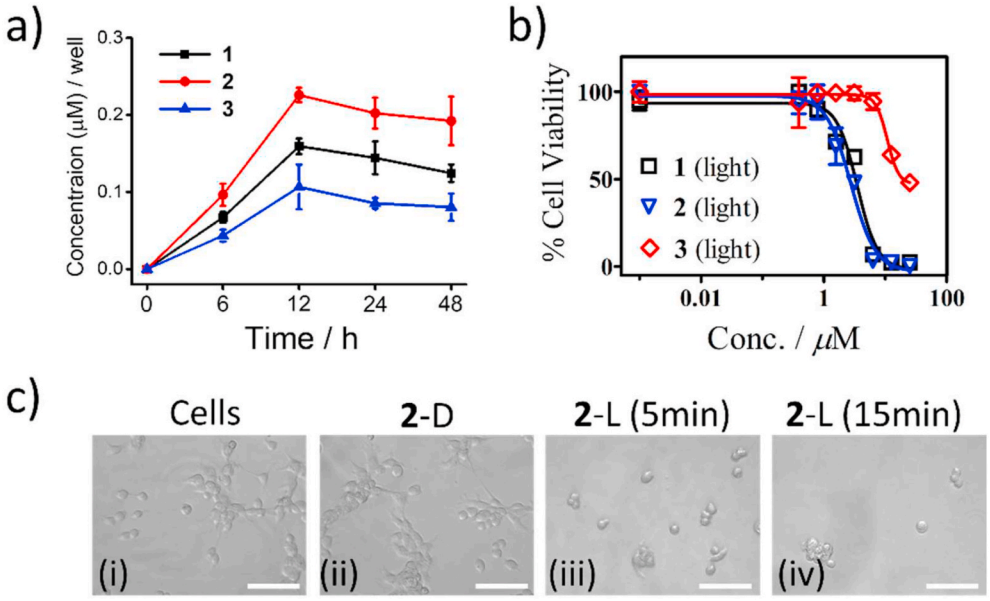

Fig. 3. (a) Time-dependent uptake of **1**–**3** at 5 μM by MCF-7 cells; uptake was measured by fluorescence spectroscopy of lysed cells and compared with calibration curves (the data shown are the means ± SD of three independent experiments); (b) Cytotoxicity of **1**–**3** in MCF-7 cells as determined by MTT assay after 12 h incubation in the dark followed by irradiation at 660 nm for 15 min with a Thorlabs M660L3 LED (280 mW cm^{-2}); (c) MCF-7 cell morphological changes observed through inverted microscopy of MCF-7 cells: (i) control cells, (ii) **2** (5 μM) treated cells in the dark, (iii) and (iv) **2** (5 μM) treated cells after photoirradiation at 660 nm for 5 and 15 min with a Thorlabs M660L3 LED (84 and 252 J cm^{-2}). [Scale bar: 200 μm].

1 and **2** compared to **3** demonstrate the effect of the heavy sulfur atoms of the thien-2-yl moiety, while the further decrease for **2** relative to **1** shows the effect of the bromine atoms [28]. The ability of **1**–**3** to generate $^1O_2$ was studied qualitatively by monitoring $^1O_2$ phosphorescence at 1270 nm [29,30] and quantitively through a comparative method by UV–visible absorption spectroscopy with 1,3-diphenylisobenzofuran (DPBF) as a $^1O_2$ scavenger [31], since **1** and **2** populate the triplet state significantly [18]. When the chlorins were excited at 420 nm close to the B band maxima, the characteristic signal of $^1O_2$ phosphorescence was observed (Fig. 2c). The singlet oxygen quantum yields of chlorins in DMF were calculated by using Rose Bengal (Φ_Δ = 0.47 in DMF [32]) as the standard. The magnitude of the Φ_Δ values follow the order: **2** > **1** > **3** (Table 1). The highest Φ_Δ value was observed for **2** due to the presence of the bromine atoms.

3.3. Photostability

During PDT, the singlet oxygen produced by the photosensitizer is known to degrade the photosensitizer itself through photobleaching [4,6]. This may reduce the efficacy of the photosensitizer and the photo-decomposed side product may cause complications. An ideal photosensitizer should be stable under the conditions that PDT is performed. Absorption spectra were measured for **1**–**3** in DMF after irradiating for up to 30 min with a Thorlabs M660L3 LED (Fig. 2d). The order of photostability follow the order: **1** (95.2%) > **2** (91.4%) > **3** (68.9%). The electron-withdrawing character of thiophene enhances the photostability of chlorins **1** and **2** [33,34].

3.4. Time-dependent cellular uptake

The time-dependent cellular uptake of chlorins (5 μM) in MCF-7 cells at different time points (6, 12, 24, and 48 h) is shown in Fig. 3a. The uptake of chlorins increases from 6 to 12 h and gradually decreased before finally saturating at 48 h. The relative order of cellular uptake at 5 μM is as follows: **2** > **1** > **3**. The level of cellular uptake is known to contribute to differences in PDT activity [35–38].

3.5. Photocytotoxicity studies in MCF-7 cells

The cytotoxicity of **1**–**3** against MCF-7 cancer cells in both the dark and upon irradiation at 660 nm with a Thorlabs M660L3 LED was assessed by MTT assay [39]. MCF-7 cells were incubated with different concentrations (0.39–25 μM) of chlorins **1**–**3** for 12 h since cellular uptake reaches a maximum at 12 h. DMSO stock solutions were used to solubilize chlorins **1**–**3** prior to being diluted further with an appropriate volume of DMEM. Even at 25 μM, the DMSO had been diluted to <0.5% during the PDT activity experiments. This has previously been found to have no significant effect on the MCF-7 cells [17,20,21]. The cells were irradiated with a Thorlabs M660L3 LED for 15 min. A separate set of chlorin treated cells were studied in parallel in the absence of light irradiation. **1**–**3** exhibited negligible dark toxicity at the tested concentrations with IC_{50} values > 25 μM (Table 2). Irradiation of MCF-7 cells pre-treated with chlorin results in significant inhibition of cell growth. Fig. 3b shows dose-dependent curves obtained against MCF-7 cells under photoirradiation. The IC_{50} values for the chlorins follows the trend **2** (2.7 μM) < **1** (3.5 μM) < **3** (15.8 μM). A comparison of the IC_{50} values for chlorins (**1**–**3**), Sn(IV) tetrathien-2-ylporphyrin (TTP) and tetraphenylporphyrin (TPP) complexes with 3-pyridyloxy (3PyO) axial ligands [20], Sn(IV) trithien-2-ylcorrole (TTC) and triphenylcorrole (TPC) complexes [24], Photofrin® and Cisplatin is made in Table 2 [40,41]. Chlorins **1** and **2** has similar photocytotoxicity properties to those reported previously for Photofrin® and the Sn(IV)TTP and Sn(IV)TTC complexes. **1** with thien-2-yl moieties show almost 3-fold

Table 2
IC_{50} values of chlorins **1**–**3** and other selected photosensitizer dyes against MCF-7 cells.

	IC_{50} (μM) Dark[a]	IC_{50} (μM) Light[b]
1	>25	3.5 (±1.1)
2	>25	2.7 (±1.0)
3	>25	15.8 (±1.2)
$[Sn(IV)TTP(3PyO)_2]$[c]	>50	5.6 (±1.1)
$[Sn(IV)TPP(3PyO)_2]$[c]	>50	18.7 (±1.1)
Sn(IV)(TTC)Cl[d]	>50	3.2 (±0.1)
Sn(IV)(TPC)Cl[d]	>50	13.1 (±0.2)
Cisplatin[e]	78.8 (±0.2)	—
Photofrin®,[f]	—	2.0 (±0.2)

[a] Cells were incubated in the dark for 24 h;[b] Incubation in the dark for 24 h followed by irradiation at 660 nm with a Thorlabs M660L3 LED (252 J cm^{-2}) for 15 min; [c]Values for Sn(IV)TTP(3PyO)$_2$ and Sn(IV)TPP(3PyO)$_2$ at 625 nm with a Thorlabs M625L3 LED (288 J cm^{-2}) for 20 min [20]; [c]Values for Sn(IV)(TTC)Cl and Sn(IV)(TPC)Cl at 660 nm with a Thorlabs M660L3 LED (504 J cm^{-2}) for 30 min [24]; [e]Values from Refs. [43]; [f]Values from Refs. [44].

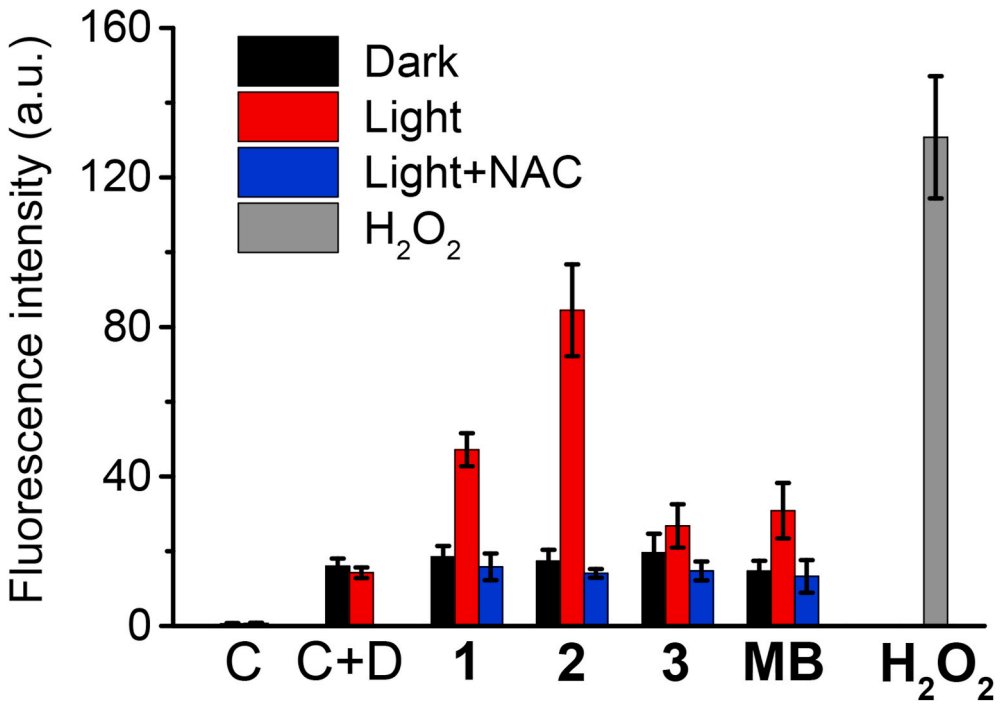

Fig. 4. ROS detection by DCFDA fluorescence assay in MCF-7 cancer cells by **1**–**3**, (Methylene blue-MB, H_2O_2 positive controls), cells (C), and cells + DCFDA (C + D) (negative control) in the dark and upon irradiation at 660 nm with and without NAC with a Thorlabs M660L3 LED. (For interpretation of the references to colour in this figure legend, the reader is referred to the Web version of this article.)

better photocytotoxicity than the phenyl analogue **3**. The observed trend in photocytotoxicity is consistent with the cellular uptake and singlet oxygen quantum yield data. The morphological change in the MCF-7 cells that is induced by **2** (5 μM) upon light irradiation treatment (5 and 15 min) was captured using an inverted microscope (Fig. 3c). Shrinkage of cells, condensed nuclei, destruction of structure, rounder morphology and a reduction in cell density were observed, which are characteristic of apoptosis [42–44]. In contrast, untreated cells and cells treated with **2** but with no light exposure did not show any morphological changes.

3.6. Intracellular ROS production (DCF-DA assay)

The intracellular ROS level was measured by DCFDA assay [45,46]. DCFHDA is a cell-permeable dye which is hydrolyzed by intracellular esterase to form 2′,7′-dichlorodihydrofluorescein (DCFH), a non-fluorescent compound. DCFH is oxidized to green fluorescent 2′, 7′-dichlorofluorescein (DCF) dye in the presence of ROS. A microplate analyzer and fluorescence microscope were used to measure DCF fluorescence at 535 nm with an excitation wavelength of 485 nm. Control experiments were performed with no chlorin present (cells only, cells + DCFDA only), with Methylene blue and H_2O_2 used as positive controls. When compared to the controls and dark treated cells, a significant increase in fluorescence intensity is observed in cells treated with photoactivated chlorins (Fig. 4). The light-induced ROS generating efficacy follows the trend **2** > **1** > **3**. These results correlate with the PDT efficacy observed for the chlorins in Table 2. The amount of ROS is reduced significantly when irradiation is carried out in the presence of NAC as a ROS scavenger. Fluorescence microscopy images of untreated MCF-7 cells and cells that were treated with **1** and **2** but with no irradiation show no green fluorescent spots (Fig. S12), in contrast to those that were irradiated with a Thorlabs M660L3 LED for 15 and 30 min at 660 nm. This further confirms that **1** and **2** produce intracellular ROS.

3.7. Antimicrobial studies

The PACT activities of **1**–**3** (Table 3) were studied against both a gram (+) bacteria, *Staphylococcus aureus*, and a gram (−) bacteria, *Escherichia coli*. To optimize the concentration for further studies, bacterial survival experiments were carried out with various concentrations of **2** under exposure to a Thorlabs M660L3 LED for 60 min with an irradiance of 280 mW cm^{-2} by a surface plating method (Fig. S13) [47, 48]. The results showed that 2.5 μM for *S. aureus* and 15 μM for *E. coli* would be suitable concentrations to enable comparison of the PACT activities of chlorins **1**–**3**. Log reduction and % cell survival values were used to quantify the results (Fig. 5a and b, and S14). In the dark, the chlorins did not show any toxicity against both *S. aureus* and *E. coli* at the concentrations studied (Fig. S14), and microbial cell viabilities were also not affected by irradiation in the absence of the photosensitizer (data not shown).

Table 3
Log reduction and percentage cell survival values for the photoinactivation effects of **1**–**3** (2.5 μM for *S. aureus* and 15 μM for *E. coli*) after 60 min irradiation with a Thorlabs M660L3 LED (280 mW cm^{-2}) at 660 nm.

	S. aureus		*E. coli*	
	Log reduction	% Cell survival	Log reduction	% Cell survival
1	7.22	0	4.98	0.8
2	7.42	0	8.34	0.0
3	1.18	96.7	0.02	64.5

In contrast, after light irradiation of **1** and **2**, *S. aureus* showed 0% cell survival with log reduction values of 7.22 and 7.42, respectively, while **3** showed 96.7% cell survival (1.18 log reduction). According to FDA regulations, log reduction values of greater than **3** classify an agent as antibacterial. Similar trends are observed against *E. coli* with the exception that **2** performed slightly better than **1** with log reduction values of 8.34 and 4.98, respectively. In marked contrast, **3** had 64.5% cell survival with a very low log reduction of 0.02. Positively charged photosensitizer dyes are normally required for gram (−) bacteria, such as *E. coli* [49]. The significant PACT activity of thien-2-yl substituted chlorins **1** and **2** (Fig. 5c and d) may be due to the effective photodynamic antibacterial and antifungal activity that has been reported

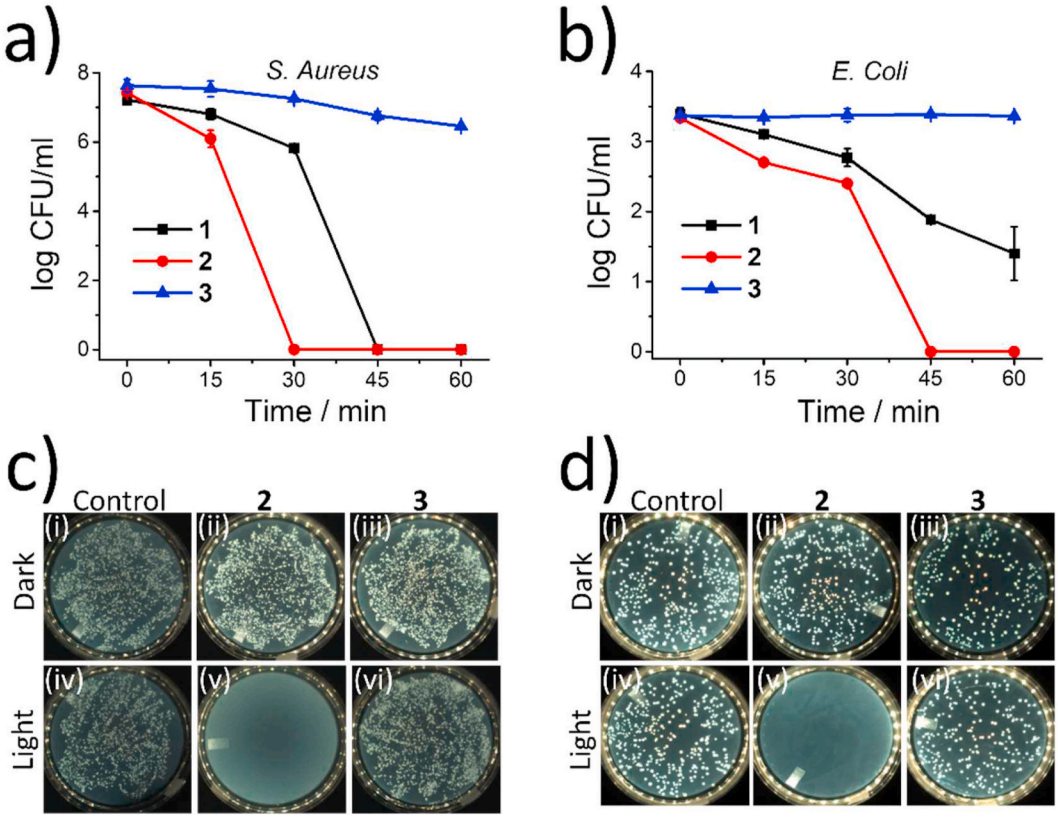

Fig. 5. Logarithmic reduction after irradiation at 660 nm with a Thorlabs M660L3 LED (280 mW cm^{-2}) of (a) *S. aureus* treated with 2.5 μM of **1**–**3**; (b) *E. coli* treated with 15 μM of **1**–**3**; (c) Images of *S. aureus* colonies formed in the dark [control (i), **2** (ii), **3** (iii)] and on irradiation at 660 nm with a Thorlabs M660L3 LED for 60 min [control (iv), **2** (v), **3** (vi)]; and, (d) Images of *E. coli* colonies formed in the dark [control (i), **2** (ii), **3** (iii)] and on irradiation at 660 nm with a Thorlabs M660L3 LED for 60 min [control (iv), **2** (v), **3** (vi)].

previously for thien-2-yl derivatives in the literature [50–53].

4. Conclusion

In conclusion, tetraarylchlorins **1**–**3** have been successfully synthesized and characterized, so that the effect of introducing *meso*-thienyl rings on the PDT and PACT activity properties could be analyzed in-depth. Thien-2-yl substituted chlorins have red-shifted absorption bands, which lie within the therapeutic window at > 650 nm and have relatively long-lived triplet states. **1** and **2** have significantly higher singlet oxygen quantum yield than their *meso*-tetraphenylchlorin analogues because of the heavy-atom effect associated with the sulfur and bromine atoms, and were found to be photostable. **2** exhibits better cellular uptake than **1** and **3** in experiments with MCF-7 cells. **1** and **2** exhibited efficient PDT activity with IC_{50} values of 3.5 and 2.7 μM against MCF-7 cells when irradiated at 660 nm with a Thorlabs M660L3 LED. The DCFDA assay provided evidence for the generation of ROS upon light irradiation. **2** was found to have better activity against *S. aureus* and *E. coli* with higher log reduction and lower percentage cell survival values. The results demonstrate that chlorin **2** has the potential to be developed further as a photosensitizer dye for PDT and PACT. Further studies are in progress on novel tetraarylchlorins with red-shifted intense Q bands that are structurally modified in a manner that enhances their aqueous solubility and lipophilicity properties to eliminate the use of DMSO stock solutions during *in vitro* cell studies.

Author statement

Balaji Babu: Investigation, Visualization, Validation, Formal Analysis, Writing- Original draft preparation. Azole Sindelo: Investigation, Formal Analysis, Validation. *John Mack*: Conceptualization, Visualization, Funding acquisition, Project administration, Supervision, Writing- Reviewing and Editing. Tebello Nyokong: Funding acquisition, Supervision, Writing- Reviewing and Editing.

Declaration of competing interest

The authors declare that they have no known competing financial interests or personal relationships that could have appeared to influence the work reported in this paper.

Acknowledgements

This work was supported by the National Research Foundation (NRF) and Department of Science and Technology (DST) of South Africa through the DST/NRF South African Research Chairs Initiative for Professor of Medicinal Chemistry and Nanotechnology to TN (uid: 62062), and an ISRR grant (uid: 119259) to JM. Photophysical measurements were enabled by equipment provided by the Laser Rental Pool Programme of the Council for Scientific and Industrial Research (CSIR) of South Africa.

Appendix A. Supplementary data

Supplementary data to this article can be found online at https://doi.org/10.1016/j.dyepig.2020.108886.

References

[1] Ethirajan M, Chen Y, Joshi P, Pandey RK. The role of porphyrin chemistry in tumor imaging and photodynamic therapy. Chem Soc Rev 2011;40:340–62. https://doi.org/10.1039/B915149B.

[2] Dąbrowski JM, Pucelik B, Regiel-Futyra A, Brindell M, Mazuryk O, Kyzioł A, Stochel G, Macyk W, Arnaut LG. Engineering of relevant photodynamic processes through structural modifications of metallotetrapyrrolic photosensitizers. Coord Chem Rev 2016;325:67–101. https://doi.org/10.1016/j.ccr.2016.06.007.

[3] Dąbrowski JM. Reactive oxygen species in photodynamic therapy: mechanisms of their generation and potentiation. Adv Inorg Chem 2017;70:343–94. https://doi.org/10.1016/bs.adioch.2017.03.002.

[4] Kwiatkowski S, Knap B, Przystupski D, Saczko J, Kędzierska E, Knap-Czop K, Kotlińska J, Michel O, Kotowski K, Kulbacka J. Photodynamic therapy-mechanisms, photosensitizers and combinations. Biomed Pharmacother 2018;106:1098–107. https://doi.org/10.1016/j.biopha.2018.07.049.

[5] Li X, Lovell JF, Yoon J, Chen X. Clinical development and potential of photothermal and photodynamic therapies for cancer. Nat Rev Clin Oncol 2020. https://doi.org/10.1038/s41571-020-0410-2.

[6] Habermeyer B, Guilard R. Some activities of PorphyChem illustrated by the applications of porphyrinoids in PDT, PIT and PDI. Photochem Photobiol Sci 2018;17:1675–90. https://doi.org/10.1039/C8PP00222C.

[7] Baskaran R, Lee J, Yang S-G. Clinical development of photodynamic agents and therapeutic applications. Biomater Res 2018;22:25. https://doi.org/10.1186/s40824-018-0140-z.

[8] Srivatsan A, Missert JR, Upadhyay SK, Pandey RK. Porphyrin-based photosensitizers and the corresponding multifunctional nanoplatforms for cancer-imaging and phototherapy. J Porphyr Phthalocyanines 2015;19:109–34. https://doi.org/10.1142/S1088424615300037.

[9] Zhang J, Jiang C, Figueiró Longo JP, Azevedo RB, Zhang H, Muehlmann LA. An updated overview on the development of new photosensitizers for anticancer photodynamic therapy. Acta Pharm Sin B 2018;8:137–46. https://doi.org/10.1016/j.apsb.2017.09.003.

[10] Allison RR, Sibata CH. Oncologic photodynamic therapy photosensitizers: a clinical review. Photodiagnosis Photodyn Ther 2010;7:61–75. https://doi.org/10.1016/j.pdpdt.2010.02.001.

[11] Laville I, Figueiredo T, Loock B, Pigaglio S, Maillard P, Grierson DS, Carrez D, Croisy A, Blais J. Synthesis, cellular internalization and photodynamic activity of glucoconjugated derivatives of tri and tetra(*meta*-hydroxyphenyl)chlorins. Bioorg Med Chem 2003;11:1643–52. https://doi.org/10.1016/S0968-0896(03)00050-6.

[12] Li X, Lee S, Yoon J. Supramolecular photosensitizers rejuvenate photodynamic therapy. Chem Soc Rev 2018;47:1174–88. https://doi.org/10.1039/C7CS00594F.

[13] Hargus JA, Fronczek FR, Vicente MGH, Smith KM. Mono-(l)-aspartylchlorin-e_6. Photochem Photobiol 2007;83:1006–15. https://doi.org/10.1111/j.1751-1097.2007.00092.x.

[14] Savary J-F, Monnier P, Fontolliet C, Mizeret J, Wagnières G, Braichotte D, van den Bergh H. Photodynamic therapy for early squamous cell carcinomas of the esophagus, bronchi, and mouth with *m*-tetra(hydroxyphenyl) chlorin. Arch. Otolaryngol Neck Surg. 1997;123:162–8. https://doi.org/10.1001/archotol.1997.01900020042006.

[15] Naim R. Photodynamische Therapie mit *m*-THPC (Foscan®). HNO 2008;56:490—492. https://doi.org/10.1007/s00106-008-1750-x.

[16] Li X, Bai H, Yang Y, Yoon J, Wang S, Zhang X. Supramolecular antibacterial materials for combatting antibiotic resistance. Adv Mater 2019;31:1805092. https://doi.org/10.1002/adma.201805092.

[17] Bolduc A, Dufresne S, Hanan GS, Skene WG. Synthesis, photophysics, and electrochemistry of thiophene-pyridine and thiophene-pyrimidine dyad comonomers. Can J Chem 2010;88:236–46. https://doi.org/10.1139/v09-166.

[18] Sadiq F, Zhao J, Hussain M, Wang Z. Effect of thiophene substitution on the intersystem crossing of arene photosensitizers. Photochem Photobiol Sci 2018;17:1794–803. https://doi.org/10.1039/C8PP00230D.

[19] Fonseca SM, Pina J, Arnaut L G, Seixas de Melo J D, Burrows H, Chattopadhyay N, Alácer L, Charas A, Morgado J, Monkman AP, Asawapirom U, Scherf U, Edge R, Navaratnam S. Triplet-state and singlet oxygen formation in fluorene-based alternating copolymers. J Phys Chem B 2006;110:8278–83. https://doi.org/10.1021/jp060251f.

[20] Babu B, Amuhaya E, Oluwole D, Prinsloo E, Mack J, Nyokong T. Preparation of NIR absorbing axial substituted tin(IV) porphyrins and their photocytotoxic properties. MedChemComm 2019;10:41–8. https://doi.org/10.1039/C8MD00373D.

[21] Ramesh J, Arunkumar C, Sujatha S. Dicationic porphyrins bearing thienyl and pyridinium moieties: synthesis, characterization, DNA interaction and cancer cell toxicity. Polyhedron 2019;170:151–9. https://doi.org/10.1016/j.poly.2019.05.042.

[22] Rangasamy S, Ju H, Um S, Oh D-C, Song JM. Mitochondria and DNA targeting of 5,10,15,20-*Tetrakis*(7-sulfonatobenzo[*b*]thiophene) porphyrin-induced photodynamic therapy via intrinsic and extrinsic apoptotic cell death. J Med Chem 2015;58:6864–74. https://doi.org/10.1021/acs.jmedchem.5b01095.

[23] Soy RC, Babu B, Oluwole DO, Nwaji N, Oyim J, Amuhaya E, Prinsloo E, Mack J, Nyokong T. Photophysicochemical properties and photodynamic therapy activity of chloroindium(III) tetraarylporphyrins and their gold nanoparticle conjugates. J Porphyr Phthalocyanines 2019;23:34–45. https://doi.org/10.1142/S1088424618501146.

[24] Babu B, Prinsloo E, Mack J, Nyokong T. Synthesis, characterization and photodynamic activity of Sn(IV) triarylcorroles with red-shifted Q bands. New J Chem 2019;43:18805–12. https://doi.org/10.1039/C9NJ03391B.

[25] Zheng X, Qian J, Tang F, Wang Z, Cao C, Zhong K. Microgel-based thermosensitive MRI contrast agent. ACS Macro Lett 2015;4:431–5. https://doi.org/10.1021/acsmacrolett.5b00058.

[26] Brückner C, Foss PCD, Sullivan JO, Pelto R, Zeller M, Birge RR, Crundwell G. Origin of the bathochromically shifted optical spectra of m*eso*-tetrathien-2′- and 3′-ylporphyrins as compared to m*eso*-tetraphenylporphyrin. Phys Chem Chem Phys 2006;8:2402–12. https://doi.org/10.1039/B600010J.

[27] Lu K, He C, Guo N, Chan C, Ni K, Weichselbaum R, Lin W. Chlorin-based nanoscale metal–organic framework systemically rejects colorectal cancers *via* synergistic photodynamic therapy and checkpoint blockade immunotherapy. J Am Chem Soc 2016;138:12502–10. https://doi.org/10.1021/jacs.6b06663.

[28] Zhao J, Xu K, Yang W, Wang Z, Zhong F. The triplet excited state of BODIPY: formation, modulation and application. Chem Soc Rev 2015;44:8904–39. https://doi.org/10.1039/C5CS00364D.

[29] Krasnovsky AA. Singlet molecular oxygen in photobiochemical systems: IR phosphorescence studies. Membr Cell Biol 1998;12:665—690.

[30] de Lucas NC, Corrêa RJ, Garden SJ, Santos G, Rodrigues R, Carvalho CEM, Ferreira SB, Netto-Ferreira JC, Ferreira VF, Miro P, Marin ML, Miranda MA. Singlet oxygen production by pyrano and furano 1,4-naphthoquinones in non-aqueous medium. Photochem Photobiol Sci 2012;11:1201–9. https://doi.org/10.1039/C2PP05412D.

[31] Dumas S, Leprêtre J-C, Lepellec A, Darmanyan A, Jardon P. Reactivity of the photoexcited forms of Hypericin, Hypocrellin A, Hypocrellin B and methylated Hypericin towards molecular oxygen: the role of charge transfer interaction. J Photochem Photobiol A 2004;163:297–306. https://doi.org/10.1016/S1010-6030(03)00343-5.

[32] Redmond RW, Gamlin JN. A compilation of singlet oxygen yields from biologically relevant molecules. Photochem Photobiol 1999;70:391–475.

[33] Huang Y-Y, Balasubramanian T, Yang E, Luo D, Diers JR, Bocian DF, Lindsey JS, Holten D, Hamblin MR. Stable synthetic bacteriochlorins for photodynamic therapy: role of dicyano peripheral groups, central metal substitution (2H, Zn, Pd), and cremophor EL delivery. ChemMedChem 2012;7:2155–67. https://doi.org/10.1002/cmdc.201200351.

[34] Dąbrowski JM, Arnaut LG, Pereira MM, Monteiro CJP, Urbańska K, Simões S, Stochel G. New halogenated water-soluble chlorin and bacteriochlorin as photostable PDT sensitizers: synthesis, spectroscopy, photophysics, and *in vitro* photosensitizing efficacy. ChemMedChem 2010;5:1770–80. https://doi.org/10.1002/cmdc.201000223.

[35] Ezzeddine R, Al-Banaw A, Tovmasyan A, Craik JD, Batinic-Haberle I, Benov LT. Effect of molecular characteristics on cellular uptake, subcellular localization, and phototoxicity of Zn(II) N-alkylpyridylporphyrins. J Biol Chem 2013;288:36579–88. https://doi.org/10.1074/JBC.M113.511642.

[36] Pucelik B, Sułek A, Drozd A, Stochel G, Pereira MM, Pinto MAS, Arnaut LG, Dąbrowski JM. Enhanced cellular uptake and photodynamic effect with amphiphilic fluorinated porphyrins: the role of sulfoester groups and the nature of reactive oxygen species. Int J Mol Sci 2020;21. https://doi.org/10.3390/ijms21082786.

[37] Mehanna S, Mansour N, Audi H, Bodman-Smith K, Mroueh MA, Taleb RI, Daher CF, Khnayzer RS. Enhanced cellular uptake and photochemotherapeutic potential of a lipophilic strained Ru(II) polypyridyl complex. RSC Adv 2019;9:17254–65. https://doi.org/10.1039/C9RA02615K.

[38] Zhu S, Wu F, Wang K, Zheng Y, Li Z, Zhang X, Wong W-K. Photocytotoxicity, cellular uptake and subcellular localization of amidinophenylporphyrins as potential photodynamic therapeutic agents: an *in vitro* cell study. Bioorg Med Chem Lett 2015;25:4513–7. https://doi.org/10.1016/j.bmcl.2015.08.072.

[39] Berridge MV, Herst PM, Tan AS. Tetrazolium dyes as tools in cell biology: new insights into their cellular reduction. Biotechnol Annu Rev 2005;11:127–52. https://doi.org/10.1016/S1387-2656(05)11004-7.

[40] Ohashi S, Kikuchi O, Tsurumaki M, Nakai Y, Kasai H, Horimatsu T, Miyamoto S, Shimizu A, Chiba T, Muto M. Preclinical validation of talaporfin sodium-mediated photodynamic therapy for esophageal squamous cell carcinoma. PloS One 2014;9:e103126. https://doi.org/10.1371/journal.pone.0103126.

[41] Yang C, Zhang H, Wang Z, Wu X, Jin Y. Mitochondria-targeted tri-triphenylphosphonium substituted *meso*-tetra(4-carboxyphenyl)porphyrin (TCPP) by conjugation with folic acid and graphene oxide for improved photodynamic therapy. J Porphyr Phthalocyanines 2019;23:1028–40. https://doi.org/10.1142/S1088424619500779.

[42] Ichikawa M, Akimoto J, Miki Y, Maeda J, Takahashi T, Fujiwara Y, Kohno M. Photodynamic therapy with talaporfin sodium induces dose- and time-dependent apoptotic cell death in malignant meningioma HKBMM cells. Photodiagnosis Photodyn Ther 2019;25:29–34. https://doi.org/10.1016/j.pdpdt.2018.10.022.

[43] Wong EL-M, Fang G-S, Che C-M, Zhu N. Highly cytotoxic iron(II) complexes with pentadentate pyridyl ligands as a new class of anti-tumor agents. Chem Commun 2005:4578–80. https://doi.org/10.1039/B507687K.

[44] Ménard F, Sol V, Ringot C, Granet R, Alves S, Morvan C Le, Queneau Y, Ono B, Krausz P. Synthesis of tetraglucosyl- and tetrapolyamine–tetrabenzoporphyrin conjugates for an application in PDT. Bioorg Med Chem 2009;17:7647–57. https://doi.org/10.1016/j.bmc.2009.09.048.

[45] Shen H-M, Shi C-Y, Shen Y, Ong C-N. Detection of elevated reactive oxygen species level in cultured rat hepatocytes treated with aflatoxin B_1. Free Radical Biol Med 1996;21:139–46. https://doi.org/10.1016/0891-5849(96)00019-6.

[46] Oparka M, Walczak J, Malinska D, van Oppen LMPE, Szczepanowska J, Koopman WJH, Wieckowski MR. Quantifying ROS levels using CM-H2DCFDA and HyPer. Methods 2016;109:3–11. https://doi.org/10.1016/j.ymeth.2016.06.008.

[47] Sindelo A, Kobayashi N, Kimura M, Nyokong T. Physicochemical and photodynamic antimicrobial chemotherapy activity of morpholine-substituted phthalocyanines: effect of point of substitution and central metal. J Photochem Photobiol A 2019;374:58–67. https://doi.org/10.1016/j.jphotochem.2019.01.025.

[48] Osifeko OL, Uddin I, Mashazi PN, Nyokong T. Physicochemical and antimicrobial photodynamic chemotherapy of unsymmetrical indium phthalocyanines alone or

in the presence of magnetic nanoparticles. New J Chem 2016;40:2710–21. https://doi.org/10.1039/C5NJ01922B.

[49] Beveridge TJ. Structures of gram-negative cell walls and their derived membrane vesicles. J Bacteriol 1999;181:4725–33. https://doi.org/10.1128/JB.181.16.4725-4733.1999.

[50] Shabangu SM, Babu B, Soy RC, Oyim J, Amuhaya E, Nyokong T. Susceptibility of Staphylococcus aureus to porphyrin-silver nanoparticle mediated photodynamic antimicrobial chemotherapy. J Lumin 2020;222:117158. https://doi.org/10.1016/j.jlumin.2020.117158.

[51] Romagnoli C, Mares D, Sacchetti G, Bruni A. The photodynamic effect of 5-(4-hydroxy-1-butinyl)-2,2'-bithienyl on dermatophytes. Mycol Res 1998;102:1519–24. https://doi.org/10.1017/s0953756298006637.

[52] Li R, Niu R, Qi J, Yuan H, Fan Y, An H, Yan W, Li H, Zhan Y, Xing C. Conjugated polythiophene for rapid, simple, and high-throughput screening of antimicrobial photosensitizers. ACS Appl Mater Interfaces 2015;7:14569–72. https://doi.org/10.1021/acsami.5b04552.

[53] Yuan H, Zhan Y, Rowan AE, Xing C, Kouwer PHJ. Biomimetic networks with enhanced photodynamic antimicrobial activity from conjugated polythiophene/polyisocyanide hybrid hydrogels. Angew Chem Int Ed 2020;59:2720–4. https://doi.org/10.1002/anie.201910979.